

Characterizing the Final Stage of Earthquake Nucleation

Changrong He¹, Lei Zhang², and Qi-Fu Chen³

¹Institute of Geology, China Earthquake Administration

²Institute of Geology

³Institute of Geology and Geophysics, Chinese Academy of Sciences

November 24, 2022

Abstract

Previous experiments and modeling on the nucleation process of an earthquake reveal accelerating slip and development of a final patch of fixed or expanding length, but whether the nucleation phase is spatially large enough to be detected in real-Earth conditions with durations long enough to be helpful is unknown. This study performed a new round of simulation of the nucleation process based on the rate-and-state friction law. Our results reveal the development of a weakening-zone core where stress releases continuously, which expands first to a dimension less than the half fault length then shrinks to a final length before re-expanding, consistent with seismicity migration before large subduction earthquakes. Onset times of the weakening-zone core are weeks before large subduction earthquakes under high loading rate but years for continental faults with loading rate below 10mm/yr. The onset of weakening-zone core is marked by fault-length-dependent slip rates >3.6-4.8 times the loading rate.

Hosted file

essoar.10508626.1.docx available at <https://authorea.com/users/533518/articles/603145-characterizing-the-final-stage-of-earthquake-nucleation>

C. He¹, L. Zhang¹, Q. Chen²

¹State Key Laboratory of Earthquake Dynamics, Institute of Geology, China Earthquake Administration, Beijing, China.

²Key Laboratory of Earth and Planetary Physics, Institute of Geology and Geophysics, Chinese Academy of Sciences, Beijing, China.

Corresponding author: Changrong He(crhe@ies.ac.cn)

Key Points:

- A weakening-zone core develops in the final stage of earthquake nucleation which expands first and then shrinks to an unstable length
- Pre-shock seismicity reveals the final weeks-long nucleation process of large subduction earthquake
- Comparison between aseismic slip rate and the loading rate helps mark the final stage of main-shock nucleation.

Abstract

Previous experiments and modeling on the nucleation process of an earthquake reveal accelerating slip and development of a final patch of fixed or expanding length, but whether the nucleation phase is spatially large enough to be detected in real-Earth conditions with durations long enough to be helpful is unknown. This study performed a new round of simulation of the nucleation process based on the rate-and-state friction law. Our results reveal the development of a weakening-zone core where stress releases continuously, which expands first to a dimension less than the half fault length then shrinks to a final length before re-expanding, consistent with seismicity migration before large subduction earthquakes. Onset times of the weakening-zone core are weeks before large subduction earthquakes under high loading rate but years for continental faults with loading rate below 10mm/yr. The onset of weakening-zone core is marked by fault-length-dependent slip rates >3.6-4.8 times the loading rate.

1 Introduction

Understanding the nucleation process of large earthquake is crucial for earthquake prediction and risk assessment as it might provide alert information on the impending earthquake. Despite differences due to roughness of simulated faults, laboratory experiments (Diterich,1978; Kato et al., 1992; Ohnaka & Shen,1999; McLaskey & Kilgore, 2013; Latour et al., 2013) and associated numerical modelling (Kaneko et al., 2016) suggest that earthquake nucleation consists of two distinct phases: an initial slow propagation phase and faster acceleration phase, both of which are creeping (aseismic) slip, followed by the final run-away rupture. In spatiotemporal views, the aseismic slip before the final run-away rupture in laboratory stick-slip cycles show expansion of the creeping region at various expansion rate associated with different time scales of milliseconds to seconds

prior to the final rupture (at a higher rate in a shorter time, Ohnaka and Kuwahara,1990; Ohnaka and Shen,1999; Dieterich, 1978; Mclasley and Kilgore, 2013, Ma and Guo, 2014; Zhuo et al., 2018, 2020). Expansion of aseismic creeping region that precedes a seismic slip has also been observed in numerical modeling of earthquake nucleation in a range of constitutive parameters and initial conditions loaded with slow tectonic stress rates (Dieterich, 1992; Rubin and Ampuero, 2005; Ampuero and Rubin,2008; Fang et al., 2010), and the expansion occurs in the final limited time before an earthquake instability, mostly in a range of 10-100s but on the order of 1000s in extreme cases where initial conditions are near the critical point(Fang et al., 2010). The latter feature in numerical models is worth revisiting under different fault parameters and initial conditions for its potential that may be useful in risk assessment. From a different perspective, a ‘meta-instability stage’ observed in laboratory stick-slip experiments has also been adopted to characterize the nucleation phase of earthquake instabilities (Ma et al.,2012), which is defined as a stage where the simulated fault passes through its peak average stress and subsequently releases stress up to the run-away instability. In spite of the explicitness of this concept, it is worth noting that the peak average stress is difficult to be observed in natural faults, and identification of such a stage in tectonic settings relies on its associated characteristics.

Despite the fact that natural observations of nucleation phases before earthquakes are difficult and remain debated (Gomberg, 2018; Ellsworth & Bulut, 2018; Acosta et al., 2019), the study of recent well-instrumented records of large earthquakes has highlighted several ruptures preceded by precursory aseismic slip, linked or not with foreshocks or aseismic transient events (Bouchon et al., 2013; Kato et al., 2012, Kato and Nakagawa, 2014; Socquet et al., 2017). However, foreshocks or aseismic slips before a main-shock can only be recognized retrospectively through statistical analysis and are not observed in many major earthquakes (Bouchon et al., 2013; Ellsworth & Bulut, 2018; Kato & Ben-Zion, 2021), especially for intraplate earthquakes (Bouchon et al., 2013). However, as seen in the case of the Iquique Mw 8.1 earthquake of Chile (April 1, 2014), acceleration of cumulative slips has been revealed via the observation of small repeating earthquakes on the seismogenic fault (Kato et al., 2016). Likewise, acceleration of cumulative slips has also been observed before the Wenchuan Mw 7.9 earthquake of China (May 12, 2008), a typical intraplate large earthquake, where the local slip rate revealed from repeating small earthquakes had accelerated to an average of $\sim 10\text{mm/year}$ (Li et al., 2011; Chen et al., 2018), equivalent to 5-10 times of the long-term average slip rate of the seismogenic fault zone (1-2mm/year, Shen et al., 2009). The acceleration of aseismic slip before an earthquake is consistent to a general feature in earthquake nucleation processes modeled with rate- and state-dependent friction laws (e.g., Dieterich, 1992) and laboratory stick-slip experiments revealed by analysis on the slip rate (Zhuo et al., 2018, 2020), but the presence of quite different accelerating aseismic slip in natural tectonic settings lasting seconds to years prior to some earthquakes indicate that the slip growth in the nucleation phase observed in experiments

and theoretical models is still a mystery.

In this study, we characterize the final stage of the nucleation process with 2D numerical simulations based on the rate- and state-dependent friction law, where the model is constrained by seismic data preceding several well-recorded interplate and intraplate large earthquakes.

2. Method

2.1. Model

Consider a straight fault in 2D infinite elastic medium (Fig. 1a), with the two ends pinned as in previous modellings by Dieterich(1992) and Fang et al.(2010).

Assume that the contacting fault surfaces are governed by the laboratory-derived rate- and state-dependent friction law (Dieterich,1979; Ruina,1983), in which the friction coefficient is controlled by the superposition of the direct (instantaneous) effect of slip rate V and the evolution effect represented by logarithm of a state variable reflecting asperity contact time,

$$\mu = \frac{\tau}{\sigma} = \mu_* + a \ln\left(\frac{V}{V_*}\right) + b \ln\left(\frac{\theta}{\theta_*}\right) \quad (1)$$

where τ is shear stress and σ is effective normal stress. a and b are positive parameters that reflect the strength of direct rate effect and the evolution effect, respectively, and they are interpreted to be intrinsically related to thermally activated Arrhenius processes under high stress. The thermally activated process can be crystalline plasticity (Nakatani, 2001; Rice et al., 2001; Brechet and Estrin, 1994) or pressure-solution creep (He et al., 2013) at asperity contacts, with concurrence of equally dominant process of cataclasis for rock materials (He et al., 2013). The evolution effect is assumed to follow the aging law,

$$\frac{d\theta}{dt} = 1 - \frac{V}{D_c} \quad (2)$$

where D_c is a characteristic slip distance, which controls the time scale of the state evolution during unsteady slip after a perturbation. The stress rate at x on the fault is calculated to be the sum of a far field stress rate $\dot{\tau}^\infty$ and the local stress rate $\dot{\tau}^e$ transferred along the fault by elastic interaction due to inhomogeneous fault slips,

$$\dot{\tau} = \dot{\tau}^\infty + \dot{\tau}^e \quad (3)$$

The local stress rate $\dot{\tau}^e$ is calculated by an integral

$$\dot{\tau}^e(x) = \int_{-\infty}^{\infty} g(x, s) V(s) ds \quad (4)$$

with the Green's function of

$$g(x, s) = \frac{G}{2\pi(1-\nu)} \frac{1}{(x-s)^2}$$

where G is shear modulus and ν is Poisson's ratio.

In the wave-number representation, equation (4) is transformed to

$$FT(\dot{\tau}^e) = -G' FT(V) \pi |\kappa|$$

where $G' = G/(1-\nu)$ for in-plane deformation mode and $G' = G$ for anti-plane case. κ is wave number, and FT is Fourier transform. So the local stress rate by elastic interaction can be calculated by inverse Fourier transform invFT,

$$\dot{\tau}^e = -invFT[G'FT(V)\pi|\kappa|] \quad (5)$$

The fault is discretized as N grids, and the Fourier transforms in (5) is calculated through a fast Fourier transform (FFT) scheme. The pinned fault ends are implemented by zero padding on the fault extension with the same dimension as the fault length. An ends-pinned fault bears relatively higher stress in the middle due to initial homogeneous slip rate and the given far-field stressing rate, and slip nucleation tends to occur in the fault middle (Dieterich,1992; Fang et al., 2010), whereas the position of slip nucleation on a periodical fault (ends not pinned) depends on spatial perturbations in the initial conditions (Rubin and Ampuero, 2005; Ampuero and Rubin, 2008). The reason for focusing on the former case in this study is to incorporate the effect of strong barriers at the two fault ends on the nucleation process. Combining equations (1) through (3) in their differential forms, numerical integration gives the evolution process of the fault model from given initial conditions with an applied loading rate. The integration was calculated with a fourth-order Runge-Kutta method using the recipe of Press et al. (1992).

2.2. Model parameters and initial conditions.

The far-field stress rate in the model is assumed to be related to the long-term average slip rate V_0 by

$$\dot{\tau}^\infty = \frac{4G'}{L} V_0 \quad (6)$$

with L as the fault length. This relation is adopted according to the average slip rate over the fault when it is driven by a homogeneously distributed stress rate (He, 2000). For convenience of use, we call V_0 as loading rate below. The shear modulus is chosen to be 40GPa, and for in-plane deformation Poisson's ratio is set to be 0.25.

All the length units in the model are scaled with D_c , and $L'_b = G' D_c / (b\sigma)$ is employed to be a reference unit of nucleation size as adopted in previous studies (Rubin and Ampuero, 2005; Fang et al., 2010). The fault is discretized into equal-spaced N grids, so the total fault length is $(N-1)L'_e$. For standard cases with $N=2^{12}$, the grid spacing is set to be $L'_e=0.1L'_b$, which is 60 times smaller than a nucleation size given by a critical size $L_{b-a} = G' D_c / [(b-a)\sigma]$ derived from the critical stiffness for instability (Rice, 1993; Ampuero and Rubin, 2008). The ratio between L'_e and L'_b changes for given fault lengths in other cases. For the parameter D_c , laboratory experiments under hydrothermal conditions show a range typically of micrometers to tens of micrometers (e.g., Blanpied et al., 1998), but it is considered to be bounded by the surface-grinding procedure in this case (Brown and Scholz,1985a). Relevant to this regard, it is noted that natural fault surfaces are fractal, in which longer wavelengths have larger asperity heights (Brown and Scholz,1985b). When subjected to the subsurface

fault-normal pressure, the surfaces form contact junctions of relatively large size, and the minimum size of these junctions are estimated to be as high as \sim cm (Scholz,1988), which is considered to control the mechanical behavior, thus the D_c parameter. Also, higher D_c values than the laboratory range are required in numerical simulations to reflect typical earthquake fracture energy of 10^6 - 10^7 J/m²(Rice, 1993). In this work we set D_c in cent-meters range to fit natural fault surfaces according to the above considerations.

Our simulation considers the nucleation process evolving from homogeneous initial stress and slip rate. The initial conditions are chosen to be in the interseismic loading phase and constrained by the limit-cycle trajectory of a spring-slider system (Fig. 1b), where the stiffness is set as the average stiffness of the fault estimated by the coefficient on the right side of equation (6). The limit cycle in Fig.1b indicate that a steady state at the loading rate V_0 is a constitutively inaccessible point.

While our main interest is on the nucleation process associated with constitutive parameters constrained by hydrothermal-condition experiments on granite at ($b/a=1.19$, $b=0.025$, Blanpied et al., 1995,1998), the effect of the degree of velocity weakening was also explored with ‘locked’ initial conditions with typical b/a values as explored in previous studies (Dieterich,1992; Rubin and Ampuero, 2005; Ampuero and Rubin, 2008; Fang et al., 2010). In all these calculations $b=0.025$ is used as the average in the velocity-weakening regime of granite. Loading rates (V_0) ranging from 1mm/yr to 85mm/yr were chosen in our calculations to simulate various tectonic settings. We mainly show the nucleation process evolved spontaneously from a homogenous ‘locked’ initial condition. As the formulation is based on quasi-static equations, the calculation is terminated when the maximum slip rate is greater than 0.1m/s.

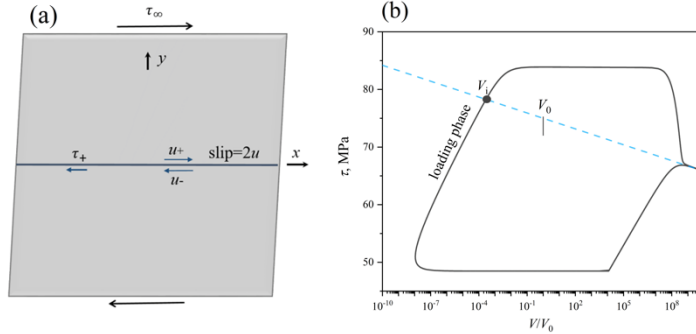


Figure 1. (a) 2D fault model in an infinite elastic medium. The fault is pinned at the two ends. (b) Trajectory of stick-slip limit cycle of a spring-slider system (black line). Initial conditions in our fault model are constrained with a point in the interseismic loading phase and arbitrarily set at the intersection with the steady-state line (ss , broken line). With loading rate V_0 and a standard fault length of 174.72km, the initial slip rate V_i is thus determined to be $\sim 2.8 \times 10^{-4}$

V_0 . The steady-state friction coefficient at V_0 is set as 0.75.

3 Results

3.1 Define distinct stages in the nucleation phase

Typical features of the nucleation phase evolved from ‘locked’ initial conditions (Fig.1b) are demonstrated with cases of various b/a values associated with $D_c=20\text{mm}$ and $V_0=83\text{mm/year}$ (Figs 2a-c). With $b/a=1.19$ (granite data) and greater, the nucleation processes show a fixed-length nucleation highlighted by the steeply-bulging slip rate profiles centered at the position of maximum slip rate (Fig.2a). The less velocity-weakening cases (lower b/a values) show expanding slip-rate profiles after the formation of a bulging nucleation length in the final short time ranging from seconds to tens of seconds(Fig.2b-c). It is of interest to compare with some cases with constitutively inaccessible initial conditions where initial stress (σ_i) and slip rate (V_i) are set at a steady state associated with the loading rate V_0 ($V_i/D_c=1$, where i denotes initial values) (cf. Fig.1b). All these latter cases show expanding slip-rate profiles after the formation of a nucleation length(Fig.2d-f), similar to calculations in previous studies (Rubin and Ampuero, 2005; Ampuero and Rubin, 2008; Fang et al., 2010). The durations of nucleation expansion ranges from $\sim 100\text{s}$ to ~ 20 days in these cases.

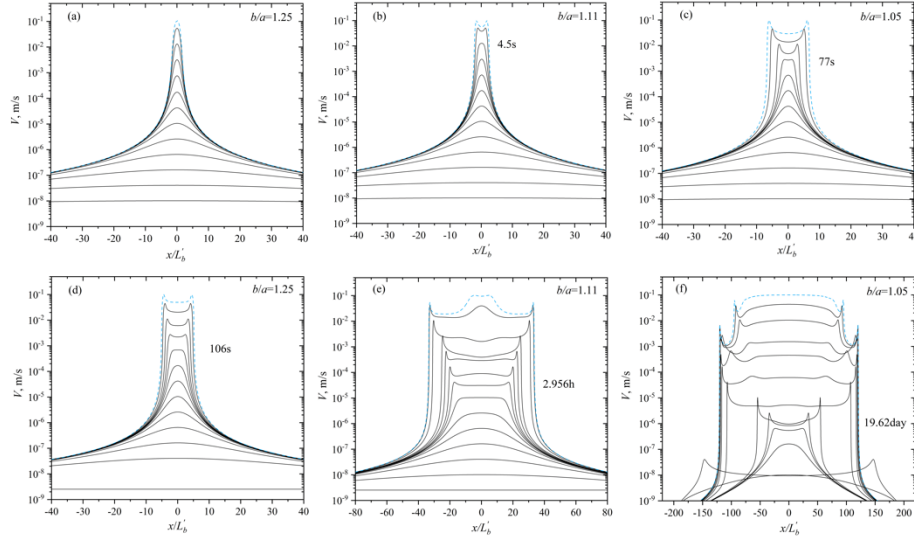


Figure 2. Evolution of slip rate profiles in the nucleation process for ‘locked’ initial conditions(a-c) and steady-state initial conditions(d-f). The time increments for the slip-rate profiles correspond to 4-times relative changes in maximum slip rate. Numbers next to the profiles are total durations of profile expansion up to the final instability. Expansion is a prominent feature for all cases of steady-state initial conditions.

With the fore-mentioned initial exploration in mind, in the following we focus only on the constitutively accessible cases with initial conditions in the ‘locked’ phase, and we first pay attention to cases with rate-dependent parameters of granite with $b/a=1.19$.

By observing the stress evolution and time series of stress profiles, the whole process can be segmented temporally into distinct stages. First, two distinct stages in the nucleation phase are revealed by observing the initial weakening and the later overall weakening in the mean stress (averaged over the whole fault). Initial peak stress occurs first at the element with maximum slip rate; and at a later point comes the peak of mean stress (Fig. 3a). The first stress peak marks the onset of local weakening while the average stress is still accumulating, thus this stage is referred to as local weakening stage (Fig. 3b). When the mean stress attains the peak value, the fault transitions from the overall stress accumulation to a stage of overall stress release. We refer to the latter stage as overall weakening stage (Fig. 3b).

By further observing the time series of stress profile, it is found that the maximum stress at the fault center ($x=0$) shifts bilaterally from a time in the overall weakening stage, and the region bracketed by the two stress shoulders expands to a final size of $\sim 2/5$ fault length for standard setting with $L_e=0.1L'_b$, forming a growing weakening zone in stress distribution (Fig. 3c). Such a delineated area does not encompass all the elements that release stress, thus it is referred to as weakening-zone core (WZcore). This core shrinks in the late stage as a result of the external elements transitioning from the stress-releasing regime back into a new stress-increasing regime. The inward migration of the core front is the result of boosted drive from the inner part with much higher slip rate in the late stage. The WZcore shrinks to a final nucleation size of $2.53\text{-}2.54L_b$ ($L_b = GD_c/[b]$) before the final run-away rupture extension, similar to the patch size of fixed length nucleation derived by Rubin & Ampuero (2005). The time of the WZcore formation to the final run-away rupture decreases with an increase in loading rate V_0 (Figs. 3c, 4a). Compared with the case of $V_0=83\text{mm/yr}$, a slower loading rate of 73mm/yr corresponds to a prolonged time of the WZcore evolution by 2.3 days (Fig.3c).

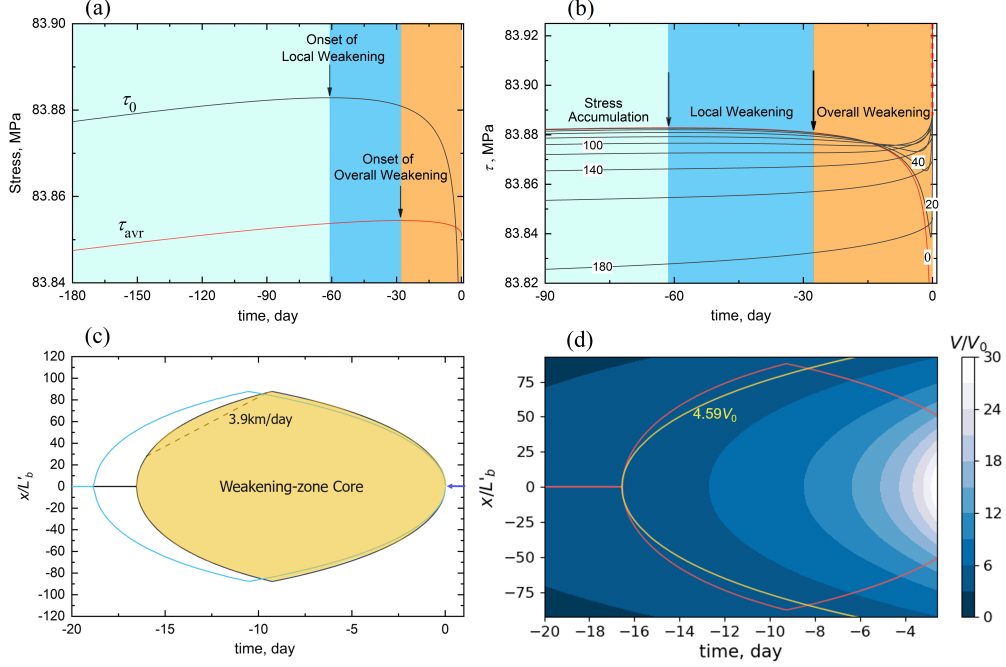


Figure 3. Features of the nucleation process with $V_0=83\text{mm/year}$ and standard constitutive parameters. (a) Initial local peak stress and subsequent peak mean stress (black arrows), which mark the onsets of local weakening and overall weakening stages (b), respectively. Numbers on stress lines in (b) are distances from the fault center in units of $L'_b = G' D_c / (\sigma b)$, in spacing of 20. (c) Spatiotemporal evolution of the weakening-zone core (colored area) revealed by early-stage shifting shoulders in stress distribution and a later shrinking process. Blue line is a result with $V_0=73\text{mm/year}$ for comparison, indicating the slowdown effect by a slower loading rate. The broken line indicates the average expansion rate of the weakening-zone core (averaged in the expanding regime with a cutoff of 8km/day). Blue arrow indicates the final WZcore length that leads to seismic instability. (d) Spatiotemporal contour map of normalized slip rate V/V_0 . Yellow line is $4.59 V_0$ associated with the onset of the WZcore, and red line the WZcore front.

3.2 Features of the WZcore in a Standard Set of Constitutive Parameters

With the rate-dependent parameter set of granite ($b/a=1.19$, $b=0.025$), $D_c=20\text{mm}$ and fault length $L=174.72\text{km}(409.5L_b)$, the feature of WZcore is described first to give a rough portrait of the nucleation process as a standard case. The expansion of the WZcore is found to be roughly associated with the area of similarly expanding higher slip rate zone with $V 4.59 V_0$ as delineated by the yellow contour in Fig. 3d (compare with the WZcore front (red line)

and the yellow contour). Thus the expansion of the WZcore is essentially a result of catching-up in slip rate along the fault. This feature is identical for all the tested loading rates, suggesting that the distribution of normalized slip rate is useful for characterizing the nucleation phase. Likewise, characteristic values of normalized maximum slip rate can be used to mark the onsets of local weakening, overall weakening, and also the beginning of the WZcore expansion. These maximum slip rates at the onsets are revealed to be $1.24 V_0$, $2.70 V_0$, and $4.59 V_0$, respectively for local weakening, overall weakening and WZcore expansion(Fig. 4a).

Since the WZcore has the property of both continuous stress release and higher slip rate, it may serve as a hot zone to drive small asperities to rupture, so it may be related to spatiotemporal evolution of small earthquakes. In this regard, it is of interest to examine the expansion rate during the WZcore growth. For a typical case with $V_0=80\text{mm/year}$, $D_c=20\text{mm}$ and fault length of 256.5km are chosen to roughly reproduce the initial time of spatial expansion of the seismicity region before the Iquique Mw 8.1 main shock of April 1, 2014, and the WZcore expansion rate is determined from the averaged slope (with a cutoff of 8km/day for initial steep curvature) to be 5.18km/day , similar to the migration rate of seismicity before the main shock (Kato and Nakagawa, 2014; Yagi et al., 2014). The expansion rate of the WZcore is found to be proportional to the loading rate V_0 , with a coefficient of $0.065 [\text{km/day}]/[\text{mm/year}]$ (Fig. 4b). The characteristic times of the nucleation process are also found to be closely related to loading rate V_0 : the start times of bulk weakening and WZcore expansion are both proportional to the reciprocal of loading rate V_0 . The start time T_{ex} of the WZcore is revealed to be $1332\text{-}2018/V_0 [\text{day}][\text{mm/yr}]$ bounded by D_c values of 20mm and 30mm used to reproduce the time scales of 2014 Iquique, Chile Mw 8.1 earthquake and the Tohoku-Oki, Japan Mw 9.0 earthquake, respectively. The start time of overall weakening is longer and is revealed to be $1.7\text{-}1.74 T_{ex}$ in these cases.

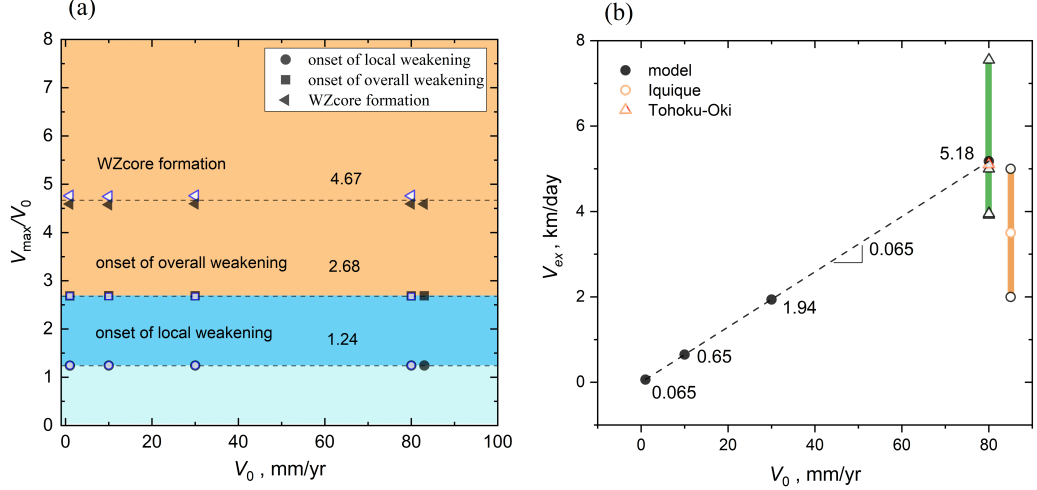


Figure 4. Characteristics of the nucleation process in standard constitutive setting: $b/a=1.19$, $b=0.025$, $D_c=20\text{mm}$. (a) Maximum slip rates at the onset of three distinctive stages: local weakening (circles), overall weakening (squares), and onset of the WZcore (triangles). Fault length of 256.5km (open symbols) and that of 174.72km (closed symbols) give similar results. (b) Expansion rate of the WZcore (V_{ex}) linearly related to the loading rate V_0 (closed circles) with a slope of 0.065 [km/day] per [mm/year]. Migration rates of seismicity during the nucleation of two megathrust earthquakes are plotted for comparison. green bar: the nucleation of 2014 Iquique, Chile Mw 8.1 earthquake (Kato and Nakagawa, 2014; Yagi et al., 2014); orange bar: nucleation of 2011 Tohoku-Oki, Japan Mw 9.0 earthquake (Kato et al., 2012). Red symbols denote the corresponding averages.

3.3 Effect of model parameters on the nucleation process

The effect of rate-dependent parameter b/a along with D_c and fault length L on the nucleation process was also explored to understand the control mechanism on the model behavior. For a given loading rate V_0 on the standard fault of 174.72km length, it is found that D_c is the first-order control on the time for the weakening-zone core formation, T_{ex} , which increases with D_c obeying a roughly linear relation (Fig.5a). b/a value also has an effect on T_{ex} , where a greater b/a value corresponds to a smaller T_{ex} (Fig.5b). From the normalized plots (Fig.5a), it is evident that T_{ex} is proportional to the reciprocal of the loading rate. With the same mechanism that controls the time scale, the average expansion rate of the WZcore is calculated to decrease with D_c but increases with V_0 , with a secondary effect of the b/a values (Fig.5c).

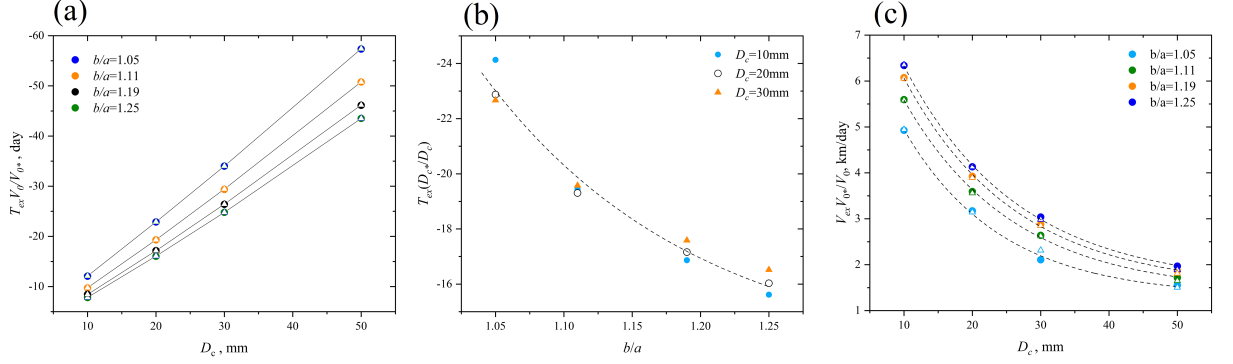


Figure 5. Effect of constitutive parameters on the feature of weakening-zone core with $L=174.72\text{km}$. (a) Onset time T_{ex} for WZcore expansion as a roughly linear relation to the characteristic slip distance D_c , where the V_0 -normalized plot indicates a linear relation between T_{ex} and reciprocal of V_0 (closed circles represent results for $V_0=80\text{mm/yr}$, and open triangles indicate results for $V_0=10\text{mm/yr}$). (b) T_{ex} is revealed to decrease with the b/a value as an exponential function. (c) Average expansion rate V_{ex} of the WZcore as functions of D_c for given b/a values, where the V_0 -normalized plot collapses to similar values for different loading rates with $V_0^*=80\text{mm/yr}$. Each expansion rate was calculated by averaging the slope over the expansion regime of the WZcore front with a cut-off at 8km/day (V_0^*/V_0) (closed circles: $V_0^*=80\text{mm/yr}$; open triangles: $V_0=10\text{mm/yr}$).

As a characteristic mark for the nucleation process, the maximum slip rate at the onset of WZcore increases with b/a but decreases with D_c for a given fault length of 174.72km , giving V_{\max}/V_0 values in a narrow range of 4.1 to 4.78 (Fig. 6).

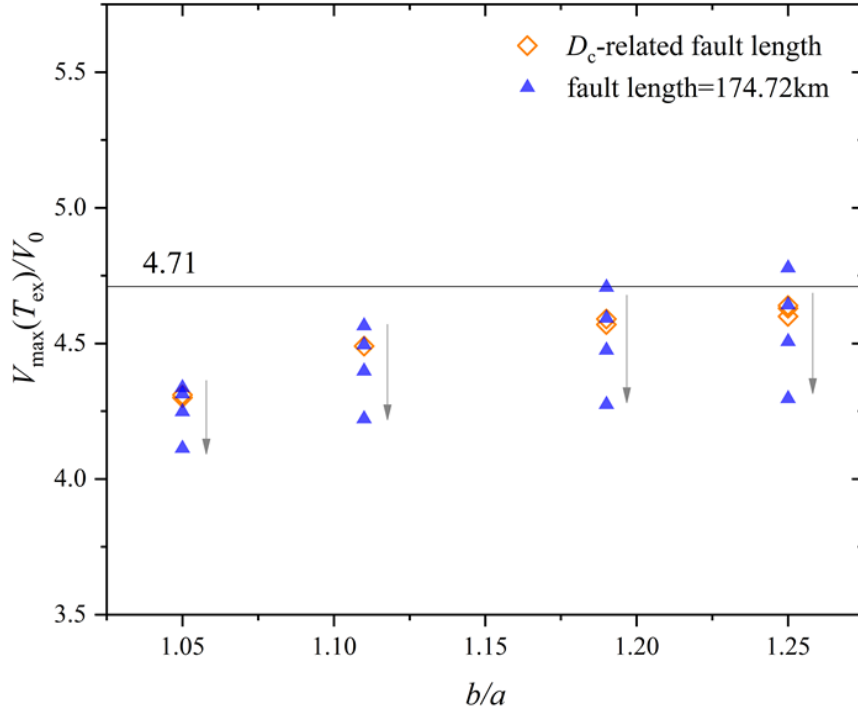


Figure 6. Maximum initial slip speeds at the onset of WZcore calculated for fault length of 174.72km and various b/a and D_c values. Arrows show the increasing direction of D_c values of 10, 20, 30 and 50mm in closed triangles. Open diamonds show the results for D_c -proportional fault length of $409.5L'_b$, plotted for comparison. V_{\max}/V_0 at T_{ex} ranges from 4.1 to 4.78 for the calculated cases.

As a shorter fault length in the model has a stronger confinement at the two ends and corresponds to a higher stressing rate (cf. eq.6 in Method), it is of interest to see how the fault length changes the model behavior. Calculations with the standard set of constitutive parameters show that a shorter fault has a longer nucleation time as represented by T_{ex} (Fig.7a). Combined effect of a longer nucleation time and a smaller maximum WZcore length results in a lower expansion rate on a shorter fault(Fig.7b). A shorter fault also corresponds to a lower maximum slip rate that marks the onset of the WZcore, as shown in Fig.7c. A typical case of a short fault of 30km length gives a $V_{\max}=3.68 V_0$, ~20% lower than a typical large fault of 230km.

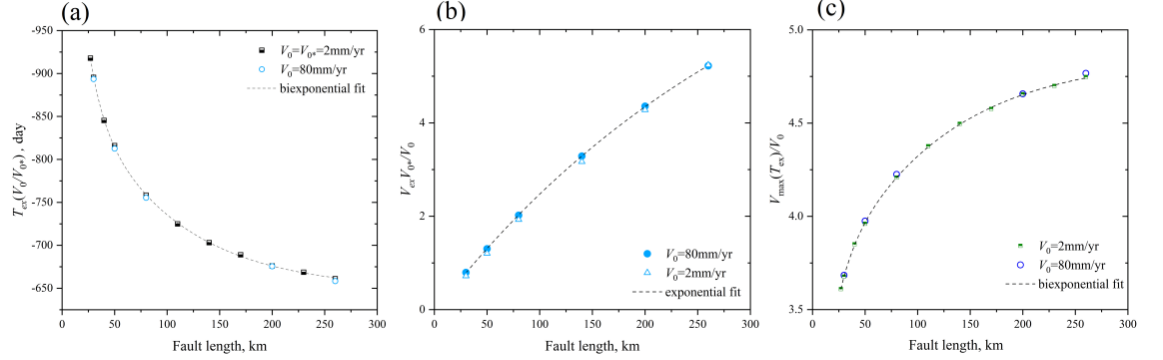
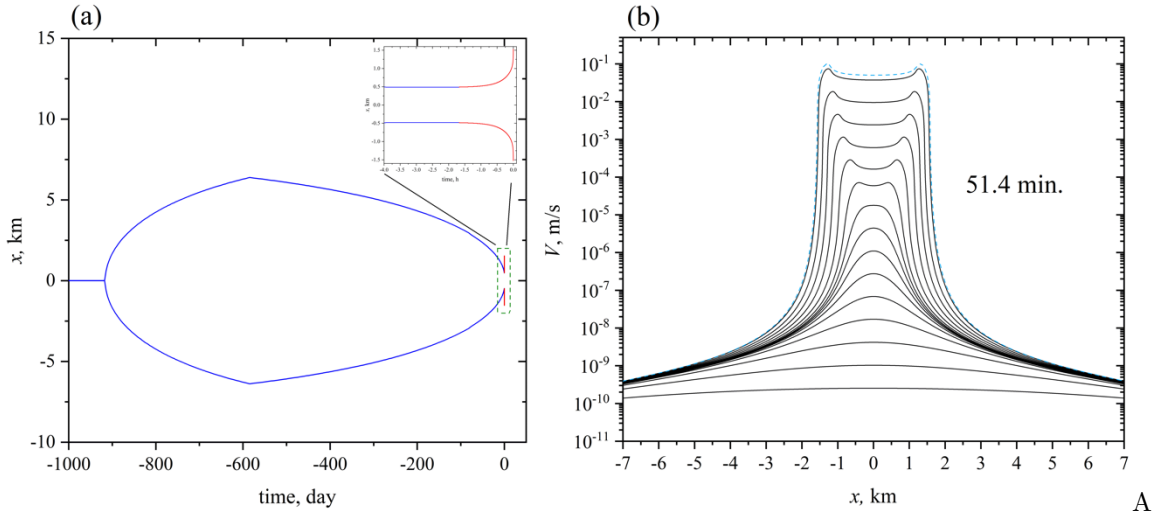


Figure 7. Effect of fault length on the onset time of WZcore (a), WZcore expansion rate(b), and maximum slip rate at the onset of WZcore (c). Data normalized by the loading rate V_0 in each plot collapse to the same function.



more outstanding effect of a short fault is found to change the evolution of the WZcore in the final short time before the earthquake instability. An example of this is demonstrated by a fault length of 27km with $V_0=2\text{mm/yr}$, where the WZcore begins to re-expand after shrinking to a fixed length of $\sim 2.27L_b$ from 1.67h to the earthquake instability(Fig.8a). Moreover, expansion in slip-rate front is also observed in this case from 51.4 min. before the final instability(Fig.8b). The re-expansion of the WZcore along with that of slip-rate front is considered to be a preshock rupture that is much slower in both slip rate ($<0.1\text{m/s}$) and propagation speed (order of kilometers /h) than in typical seismic ruptures.

Figure 8. Evolution of the WZcore of a short fault of 27km length with $V_0=2\text{mm/yr}$ and standard constitutive parameters (a) and the corresponding

slip-rate profiles(b). Inset in (a) shows the details of the slow pre-shock rupture propagation after shrinking to the minimum length. Number next to the slip-rate profiles indicates the onset time of profile expansion to the earthquake instability.

4 Discussion and Conclusion

4.1 Relevance to spatiotemporal migration of seismicity before the main shock

By observing the stages of the nucleation process, it is noted that focusing on the bulk-weakening stage is critical for practical strategy in prediction of the final instability. The “meta-instability” stage proposed by Ma et al. (2012) in laboratory experiment refers to the same stage. An important feature of this stage is the formation of the WZcore and its expansion-contraction evolution up to the earthquake instability (Fig. 3c). As the WZcore is a region that releases elastic potential energy (by stress release) at higher slip rates than the surrounding (Fig. 3d), it is here considered to be related to the aseismic-slip-driven seismicity before the main shock. Migration of seismicity before recent interplate large earthquakes at subduction zones in Japan (2011 Tohoku-Oki Mw 9.0 earthquake, Kato et al., 2012) and Chile (2014 Iquique Mw 8.1 earthquake, Kato and Nakagawa, 2014; Yagi et al., 2014) have been revealed to have an expanding zone of seismicity with a migration rate of 2-5km/day (Fig. 4b), and tend to shrink after reaching to a lateral distance of ~55km (Fig. 9a), consistent with our numerical model with $D_c=20\text{mm}$, $L=256.5\text{km}$ and $V_0=80\text{mm/yr}$ (solid line in Fig. 9a). As stress transfer from asperity ruptures may have an effect on the WZcore evolution, the fitting parameters D_c and fault length are considered to be the effective values suitable for the overall process here.

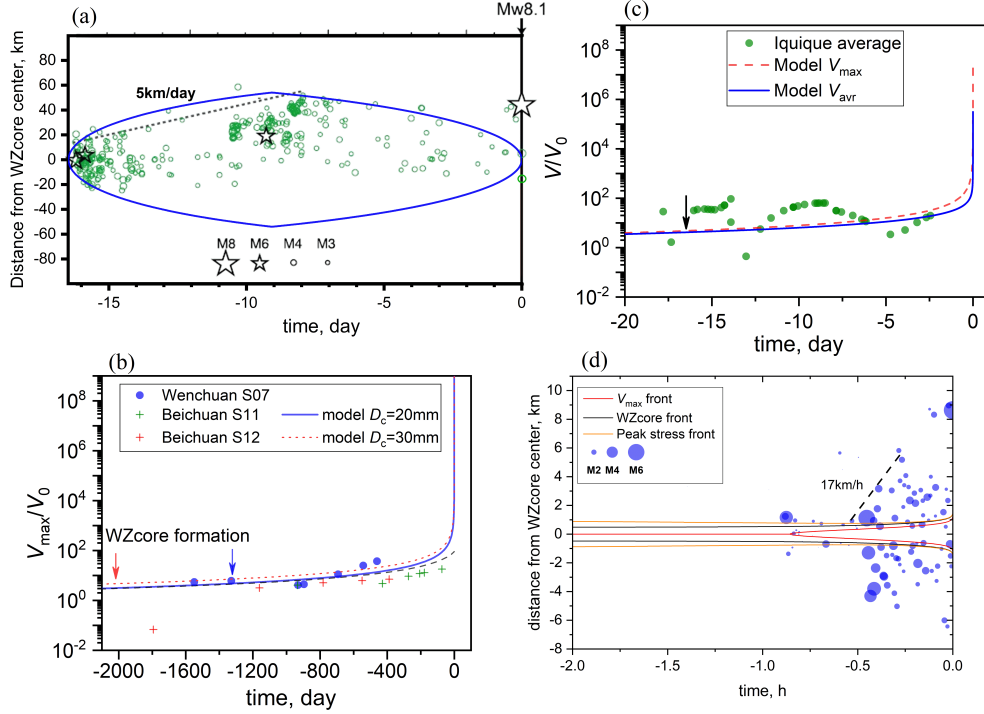


Figure 9. The nucleation processes of 2014 Iquique Mw 8.1 earthquake and 2008 Wenchuan Mw 7.9 earthquake, along with 2021 Yangbi Ms 6.4 earthquake. (a) Evolution of the weakening-zone core (area in blue line) calculated for 2014 Iquique M_w 8.1 earthquake. Plot of foreshocks of magnitude M3 are modified from Yagi et al.(2014). Dotted line: migration rate of the seismicity front. (b) Model maximum slip rate at fault center (blue line) compared with slip rates inferred from repeating microearthquakes on Yingxiu-Beichuan fault (dots and crosses). Black broken line denotes the model slip rate at a distance of 18.8 km from the WZcore center. S07-12 are numbers of repeater sequences. Blue and red arrows indicate the points of WZcore formation by model prediction with D_c of 20mm and 30mm, respectively. (c) Model average slip rate (blue line) compared with average fault slip rate (green dots) inferred from repeaters before the Iquique earthquake. (d) Pre-shock seismicity in the final 1 hour before the Yangbi Ms 6.4 earthquake compared with the expanding fronts of maximum slip rate(red line), WZcore(black line), and maximum stress(yellow line), respectively. Along-strike positions of the small earthquakes are data from Wang et al.(2021). Loading rates are set to 80mm/yr (Demets et al.,1990) and 1mm/yr (Shen et al., 2009) for Iquique earthquake and Wenchuan earthquake, respectively.

4.2 Recognize the final stage of nucleation by estimates of slip rate: 2008 Wenchuan and 2014 Iquique cases

In addition to migration of seismicity, estimates of the slip rate in the WZcore can also be used to identify the final stage of nucleation. This feature is especially useful when the nucleation duration is very long. The slip rate can be estimated by repeated microearthquakes (Nadeau and McEvilly, 1999). As an extreme case with a tectonic loading of $\sim 1\text{mm/yr}$ in the nucleation of 2008 Wenchuan Mw 7.9 earthquake (Shen et al., 2009), repeated microearthquakes at seismogenic depth before the main shock have been observed, and the time series of cumulative slips reveal the in-situ slip rate as high as $\sim 37\text{ mm/yr}$ at Wenchuan section ~ 1.26 year before the final earthquake instability (Li et al., 2011; Chen and Li, 2018). With D_c values constrained by time scales of Iquique Mw 8.1 earthquake ($D_c=20\text{mm}$) and Tohoku-Oki Mw 9.0 earthquake ($D_c=30\text{mm}$), the nucleation model predicts quite similar slip rate evolution revealed by the S07 repeater sequence in the Wenchuan section (Fig. 9b). A lower maximum slip rate of $\sim 18\text{ mm/yr}$ has also been revealed by a repeater sequence (sequence S11 in their data set) in Beichuan section ~ 73 days before the Wenchuan earthquake, indicating that it is also in the final stage of nucleation since the maximum slip rate was significantly higher than $5V_0$ (cf. Fig. 3d). However, the slip rate revealed by S11 sequence was well below the model predictions (Fig. 9b), implying that the seismic slip at Beichuan section is likely to have been triggered by the rupture propagation started from the Wenchuan section.

Similarly, observation on repeated earthquakes before the 2014 Iquique, Chile Mw 8.1 main shock reveals average slip rates ranging from 36mm/yr to 7.4m/yr (Kato et al., 2016), wobbling around the model-predicted slip rate during the final 18 days to the main shock (Fig. 9c).

Although the evolution of aseismic fault slip in the nucleation model is smooth, it does have the characteristics similar to a ‘step-like increase’ in fault slip as interpreted for the nucleation phases of large subduction earthquakes by Kato and Ben-Zion(2021) : beyond the time when the weakening-zone core is formed, it expands and plays a role of potential-energy source, and the slip rate distribution evolves to a level much higher than the tectonic loading rate. The evolution of this special core can drive tiny asperities in it to rupture and cause more seismic slips. Thus it is intrinsically plausible that the step-like aseismic slip inferred from repeaters in the weeks-long foreshock sequences before the Iquique earthquake correspond to the weakening-zone core evolution revealed in the model calculation.

4.3 Possible association between slow rupture propagation and increased seismicity

The slow rupture propagation before the main shock on a short fault (cf. **3.3**) is speculated here to drive the asperities on its way of propagation and outward surroundings to rupture. The 2021 Yangbi Ms6.4 earthquake on a 27km-long fault(Su et al., 2021; Wang et al., 2021) had a step-like increase in seismicity ~ 52 minutes before the main shock. In the final time of ~ 30 minutes, the increase of seismicity accelerated slowly, and its front expanded outwards with a rate of $\sim 17\text{km/h}$ (Wang et al., 2021). As calculated in **3.3**, the onset time of

step-like increase of seismicity coincides with the branching point of slip-rate front, and the starting point of the seismicity expansion occurred at a similar time when the stress front begins to expand (Figure 9d). Despite the coincidences in time, the significantly broader region of seismicity migration cannot be straightforwardly explained by direct comparison, thus there must be additional mechanisms that remain to be explored, which could be stress transfers from asperity ruptures combined with the driving from aseismic slip to trigger more seismic slips, making the seismicity front expand more.

3.4 Concluding remarks

We performed a suite of numerical simulations on earthquake nucleation based on the rate-and-state friction law. By observing the time series of stress profiles in the nucleation process, we reveal the development of a weakening-zone core, which expands first and then shrinks, similar to weeks-long seismicity migration before large subduction earthquakes. An associated feature of the weakening-zone core is the significantly higher slip rate compared with the loading rate by 3.6-4.8 times, depending on the fault length. The latter feature can be used to identify the final stage of earthquake nucleation of long durations by observing the aseismic slip rate through repeated earthquakes before the main shock. From the above comparison with several earthquakes, it can be seen that these features might be useful in identifying the final stage of earthquake nucleation, and the level of aseismic slip rate is a general mark of this stage.

Acknowledgments

We thank Guanshui Xu and Xi Zhang for discussions in the early stage of this research. This study was supported by National Key R&D Program of China under grant No. 2018YFC1503301.

Open Research

Our model description, calculation results and comparison with seismic data in high-resolution figures and legends are available in this in-text data citation reference: He, Zhang and Chen (2021) [CC BY 4.0].

References

- Acosta, M., Passelègue, F. X., Schubnel, A., Madariaga, R., & Violay, M. (2019). Can precursory moment release scale with earthquake magnitude? A view from the laboratory. *Geophysical Research Letters*, 46, 12,927–12,937. <https://doi.org/10.1029/2019GL084744>
- Ampuero, J. P., & Rubin, A. M. (2008). Earthquake nucleation on rate and state faults—Aging and slip laws. *Journal of Geophysical Research: Solid Earth*, 113(B1).

- Bouchon, M., Durand, V., Marsan, D., Karabulut, H. & Schmittbuhl, J. The long precursory phase of most large interplate earthquakes. *Nat. Geosci.* 6, 299–302 (2013).
- Brown, S. R., & Scholz, C. H. (1985a). Closure of random elastic surfaces in contact. *Journal of Geophysical Research: Solid Earth*, 90(B7), 5531-5545.
- Brown, S. R., & Scholz, C. H. (1985b). Broad bandwidth study of the topography of natural rock surfaces. *Journal of Geophysical Research: Solid Earth*, 90(B14), 12575-12582.
- Chen, Q. F., & Li, L. (2018). Deep deformation of the Longmenshan fault zone related to the 2008 Wenchuan earthquake. *Chinese Science Bulletin (in Chinese with English abstract)*, 63(19), 1917-1933.
- DeMets, C., Gordon, R. G., Argus, D. F., & Stein, S. (1990). Current plate motions. *Geophysical Journal International*, 101(2), 425-478.
- Dieterich, J. H. (1978). Preseismic fault slip and earthquake prediction. *Journal of Geophysical Research: Solid Earth*, 83(B8), 3940-3948.
- Dieterich, J. H. (1979). Modelling of rock friction: 1. Experimental results and constitutive equations, *J. Geophys. Res.*, 84, 2161-2168.
- Dieterich, J. H. (1992), Earthquake nucleation on faults with rate and state-dependent strength, *Tectonophysics*, 211, 115-134.
- Ellsworth, W. L. & Bulut, F. (2018) Nucleation of the 1999 Izmit earthquake by a triggered cascade of foreshocks. *Nat. Geosci.* 11, 531-535. <https://doi.org/10.1038/s41561-018-0145-1>.
- Fang, Z., Dieterich, J. H., & Xu, G. (2010). Effect of initial conditions and loading path on earthquake nucleation. *Journal of Geophysical Research: Solid Earth*, 115(B6).
- Gomberg, J. (2018). Unsettled earthquake nucleation. *Nature Geoscience*, 11(7), 463-464.
- He, C. (2000). Numerical simulation of earthquake nucleation and precursory process in slipping fault planes. *Earthquake Research in China*, 16(1), 1-11.
- He, C., Zhang, L., and Chen, Q.(2021), Method and results of a 2D numerical simulation on earthquake nucleation. Retrieved from: <https://doi.org/10.6084/m9.figshare.16778788>.
- Kaneko, Y., Nielsen, S. B. & Carpenter, B. M. The onset of laboratory earthquakes explained by nucleating rupture on a rate-and-state fault. *J. Geophys. Res. Solid Earth* 121, 6071–6091 (2016).
- Kato, A., Ben-Zion, Y. The generation of large earthquakes. *Nat Rev Earth Environ* 2, 26–39 (2021). <https://doi.org/10.1038/s43017-020-00108-w>
- Kato, A., Obara, K., Igarashi, T., Tsuruoka, H., Nakagawa, S., & Hirata, N. (2012). Propagation of slow slip leading up to the 2011 Mw 9.0 Tohoku-Oki

earthquake. *Science*, 335(6069), 705-708.

Kato, A., & Nakagawa, S. (2014). Multiple slow-slip events during a foreshock sequence of the 2014 Iquique, Chile Mw 8.1 earthquake. *Geophysical Research Letters*, 41(15), 5420-5427.

Kato, A., Fukuda, J. I., Kumazawa, T., & Nakagawa, S. (2016). Accelerated nucleation of the 2014 Iquique, Chile Mw 8.2 earthquake. *Scientific reports*, 6, 24792.

Kato, N., Yamamoto, K., Yamamoto, H., & Hirasawa, T. (1992). Strain-rate effect on frictional strength and the slip nucleation process. *Tectonophysics*, 211(1-4), 269-282.

Kirkpatrick, J. D., et al. (2015), Structure and lithology of the Japan Trench subduction plate boundary fault, *Tectonics*, 34, 53–69, doi:10.1002/2014TC003695.

Latour, S., Schubnel, A., Nielsen, S., Madariaga, R. & Vinciguerra, S. (2013), Characterization of nucleation during laboratory earthquakes. *Geophys. Res. Lett.* 40, 5064–5069.

Li, L., Chen, Q. F., Niu, F., & Su, J. (2011). Deep slip rates along the Longmen Shan fault zone estimated from repeating microearthquakes. *Journal of Geophysical Research: Solid Earth*, 116(B9).

Ma, J., Sherman, S. I., & Guo, Y. (2012). Identification of meta-unstable stress state based on experimental study of evolution of the temperature field during stick-slip instability on a 5 bending fault. *Science China Earth Sciences*, 55(6), 869-881.

Ma, J., & Guo, Y. S. (2014). Accelerated synergism prior to fault instability: evidence from laboratory experiments and an earthquake case (in Chinese with English abstract). *Seismol. Geol.* 36(3), 547-561.

McLaskey, G. C., & Kilgore, B. D. (2013). Foreshocks during the nucleation of stick-slip instability. *Journal of Geophysical Research: Solid Earth*, 118(6), 2982-2997.

Nadeau, R. M., & McEvilly, T. V. (1999). Fault slip rates at depth from recurrence intervals of repeating microearthquakes. *Science*, 285(5428), 718-721.

Ohnaka, M., & Kuwahara, Y. (1990). Characteristic features of local breakdown near a crack-tip in the transition zone from nucleation to unstable rupture during stick-slip shear failure. *Tectonophysics*, 175(1-3), 197-220.

Ohnaka, M., & Shen, L. F. (1999). Scaling of the shear rupture process from nucleation to dynamic propagation: Implications of geometric irregularity of the rupturing surfaces. *Journal of Geophysical Research: Solid Earth*, 104(B1), 817-844.

Rice, J. R. (1993). Spatio-temporal complexity of slip on a fault. *Journal of Geophysical Research: Solid Earth*, 98(B6), 9885-9907.

- Rubin, A. M., & Ampuero, J. P. (2005). Earthquake nucleation on (aging) rate and state faults. *Journal of Geophysical Research: Solid Earth*, 110(B11).
- Ruina, A. (1983), Slip instability and state variable friction law, *J. Geophys Res.* 88,10359–10370.
- Scholz, C. H. (1988). The critical slip distance for seismic faulting. *Nature*, 336(6201), 761-763.
- Shen, Z. K., Sun, J., Zhang, P., Wan, Y., Wang, M., Bürgmann, R., ... & Wang, Q. (2009). Slip maxima at fault junctions and rupturing of barriers during the 2008 Wenchuan earthquake. *Nature geoscience*, 2(10), 718-724.
- Socquet, A., Valdes, J. P., Jara, J., Cotton, F., Walpersdorf, A., Cotte, N., et al. (2017). An 8-month slow slip event triggers progressive nucleation of the 2014 Chile megathrust. *Geophysical Research Letters*, 44, 4046–4053. <https://doi.org/10.1002/2017GL073023>
- Su, J., Liu, J., Zhang, Y. et al. (2021). High resolution earthquake catalog building for the 21 May 2021 Yangbi Yunnan, Ms6.4 earthquake sequence using deep-learning phase picker. *Chinese J. Geophys.* (in Chinese with English abstract), 64(8), 2647-2656, doi:10.6038/cjg2021O0530.
- Wang, K., Jin, M., Huang, Y., et al.(2021), Temporal and spacial evolution of the 2021 Yangbi(Yunnan) Ms6.4 earthquake sequence, *Seismology and Geology* (in Chinese with English abstract), 43, 1030-1039, doi:10.3969/j.issn.0253.4967.2021.04-019.
- Yagi, Y., Okuwaki, R., Enescu, B., Hirano, S., Yamagami, Y., Endo, S., & Komoro, T. (2014). Rupture process of the 2014 Iquique Chile earthquake in relation with the foreshock activity. *Geophysical Research Letters*, 41(12), 4201-4206.
- Zhuo, Y. Q., Liu, P., Chen, S., Guo, Y., & Ma, J. (2018). Laboratory observations of tremor-like events generated during preslip. *Geophysical Research Letters*, 45(14), 6926-6934.
- Zhuo, Y. Q., Guo, Y., Chen, S., & Ji, Y. (2020). Laboratory study on the effects of fault waviness on granodiorite stick-slip instabilities. *Geophysical Journal International*, 221(2), 1281-1291.